Available online at www.sciencedirect.com

ScienceDirect

Acta Materialia 93 (2015) 246–255

Acta MATERIALIA

www.elsevier.com/locate/actamat

Study of 3-D stress development in parent and twin pairs of a hexagonal close-packed polycrystal: Part I – *in-situ* three-dimensional synchrotron X-ray diffraction measurement

Hamidreza Abdolvand,[a,d,*] Marta Majkut,[b,d] Jette Oddershede,[b] Jonathan P. Wright[c] and Mark R. Daymond[d]

[a]*Department of Materials, University of Oxford, Parks Road, Oxford OX1 3PH, UK*
[b]*NEXMAP, Department of Physics, Technical University of Denmark, Fysikvej, 2800 Kgs. Lyngby, Denmark*
[c]*ESRF, 71 Avenue Des Martyrs, 38000 Grenoble, France*
[d]*Department of Mechanical and Materials Engineering, Queen's University, Nicol Hall, 60 Union Street, Kingston, Ontario K7L 3N6, Canada*

Abstract—High anisotropy in the elastic and plastic properties of hexagonal close-packed (hcp) structured metals not only results in drastic stress variation across grain boundaries, but also heterogeneous distributions within grains. Understanding the mechanism of load sharing between different grains becomes more complicated when deformation twinning plays a significant role in accommodating an externally applied load. In this paper, a comprehensive study of stress development in a coarse grained strongly textured hcp polycrystal Zircaloy-2, is given using three-dimensional X-ray diffraction (3DXRD) microscopy. In-situ uniaxial straining was carried out at seven steps up to 2.7% in the macroscopic direction that favors twin formation, while center-of-mass position, crystallographic orientation, elastic strain, stress, and relative volume of each grain were measured. This information was used to reconstruct the 3D microstructure and statistically study neighborhood effects on the load sharing. The investigated volume of the sample contained 6132 grains initially, yet as a result of twin formation, 9724 grains were measured in the same volume at the last loading step. It is shown that the most favored (highest Schmid factor) twin variant contributes the most to the twin number fraction; however, if the measured local stress within each grain is used for the calculation of Schmid factor, the contribution of other variants is relatively independent of Schmid factor.

Keywords: 3DXRD; Twin; Hexagonal close-packed crystal

1. Introduction

Understanding deformation mechanisms in polycrystalline materials has been an active area of research for a long time. Zircaloy-2, a dilute alloy of zirconium with an hcp crystal structure is a material that has been extensively used in structural components and cladding in nuclear reactors; it has a relatively low crystal symmetry and exhibits different modes of plastic deformation when loaded in different directions relative to the source texture [1,2]. Under tension along the *c*-axis of the crystal, the lack of easy slip systems results in reorientation of a discrete part of the grain by mechanical twinning. It is reported that formation of twins can affect crack nucleation [3,4] and the stress field around the crack tip [5–9]. Hence, understanding the mechanism of load sharing between grains and twins could effectively lead to a better insight into the analysis of crack initiation and propagation and a better estimation of the lifetime of in-service components.

Various experimental methods have been used to study deformation in individual grains [10] or families of grains [11,12] in hcp crystals. At the lower scale, the strain gradient across a grain containing twins embedded in the bulk of a polycrystalline Mg AZ31 sample was studied by Balogh et al. [13]. Using the differential-aperture X-ray microscopy method, high stress gradients close to the twin boundary were observed. A similar experiment was performed by Aydiner et al. [14] where they showed that the normal stresses at the twin boundary in a single parent and twin pair are identical. A more detailed description of the twin nucleation mechanism in another hcp polycrystal, a commercially pure titanium (CPTi) sample, was given by Bieler et al. [15] where the effects of soft and hard neighbors on the variant selection occurring during twin nucleation in three twinned grains was studied using 3DXRD. At a larger

* Corresponding author at: Department of Materials, University of Oxford, Parks Road, Oxford OX1 3PH, UK; e-mail addresses: hamidreza.abdolvand@materials.ox.ac.uk; hamid.abdolvand@gmail.com

http://dx.doi.org/10.1016/j.actamat.2015.04.020
1359-6462/

scale, a comprehensive 2D statistical study of grain size, orientation, and boundary lengths on twin nucleation in Zr and Mg samples was given by Capolungo et al. [16] and Beyerlein et al. [17], respectively, using Electron-Backscattered Diffraction (EBSD). Also, neutron diffraction measurements have revealed that stresses in some measured directions are relaxed in newly born twins in comparison to their parent grains [18,19]. Although neutron diffraction provides a good statistical picture of interaction between all twin and parent grains, the stress tensor within each twin and its specific parent grain has not yet been measured statistically.

Studies of the interaction between twin and parent pairs have indicated that neighboring grains can play a significant role in stress development inside the twin or even in the thickening of twins [10,14,15,20]. Hence, a thorough understanding of deformation twinning requires a high population of twinned grains, where each grain experiences a different neighboring arrangement. Such a measurement can now be done by 3DXRD, a novel method that allows measuring of full stress tensors in a high population of grains quickly and non-destructively [21,22]. With 3DXRD, clusters of grains are illuminated simultaneously and the diffracted signals from these grains are measured with a detector while the sample is rotated about an axis perpendicular to the beam. Center-of-mass position, volume, crystallographic orientation, average elastic strain (and hence stress) within each grain are among the parameters that can be measured using 3DXRD. Diffraction Contrast Tomography (DCT) is another method that has been used to study deformation in large populations of grains. DCT has a similar characteristic to 3DXRD, yet the sample has to be close to the detector, and consequently it is difficult to extract stress and strain from DCT with sufficient accuracy [23–25].

In this study, deformation in each grain of Zircaloy-2 is studied, as an example of a polycrystalline hcp material that twins. A statistical analysis of stress development in each parent and twin is provided. Stress development in each grain during *in-situ* uni-axial loading along the direction that favors mechanical twinning is measured using 3DXRD. We note that this is the first time such a statistical set of data has been collected in 3D; previous 3D work has examined only a handful (3 or fewer) twinned grains [13–15]. In the first part of this study, the 3D microstructure of the investigated volume is generated based on the measured center of mass and volume of each grain, and the effects of microstructure on stress development in the parent and twin grains are studied statistically. In the second part [26], the measured 3D microstructure is imported into Abaqus [27] and simulated using a crystal plasticity finite element model [2,28] to study local effects on the behavior of each individual parent and twin pair and to provide complementary information about local twin-parent pair interaction.

2. Experimental set up

2.1. Material

The material used was a plate taken from the mid thickness of a warm rolled Zircaloy-2 slab, a place with uniform texture. This slab has been well characterized by the authors with *in-situ* neutron diffraction experiments [29] and various types of crystal plasticity modeling [2,30]. The slab has an hcp crystal structure at room temperature with nominal composition Zr, 1.2–1.7 wt% Sn, 0.07–0.2 wt% Fe, 0.05–0.15 wt% Cr, 0.03–0.08 wt% Ni, 1400 ppm oxygen [31]. A previous texture measurement on the slab indicated that most of the basal plane normals are oriented toward the Normal Direction (ND) with more distribution toward the Transverse Direction (TD) than the Rolling Direction (RD) [29]. In order to avoid overlapping of diffraction spots from different grains, coarse grained samples are favorable for 3DXRD. The grain size of the starting plate was ~13 μm, hence, in order to produce potential grain nucleation sites, the plate was cold-rolled to 10% (compression along the previous rolling direction) and then heat treated at 720 °C for 48 h, in an argon environment, to prevent oxide layer formation. The resulting material has equiaxed grains with an average grain size of ~50 μm. An EBSD map of the initial material and the corresponding pole figure are shown in Fig. 1(a) and (b). Tensile dog-bone samples with 10 mm gauge length and rectangular cross sections (see Fig. 1(c)) were then made by carefully machining the heat treated plate using an electric discharge machine. In order to minimize the effect of surface residual stresses associated with machining, the samples where mechanically polished down to 1200 grid on both ND/RD sides, and then with 6, 3, and 1 μm diamond paste. Subsequent attack polishing of the sample was performed several times with a solution of 5% H_2O_2, 5% HNO_3, 5% HF, and 85% H_2O for 15 s until a shiny surface with no visible scratches resulted. The final gauge cross section of the samples before the 3DXRD experiment was $0.842 \times 0.877\ mm^2$.

2.2. In-situ synchrotron experiment

Diffraction of high energy X-rays was used to study deformation in individual grains while a tensile load was applied. The experiment was carried out at beamline ID11 of the European Synchrotron Radiation Facility (ESRF). One sample was used for the measurement, over a period of approximately one week. The prepared dog bone sample was mounted in an Admet tensile rig where uniaxial tensile load was applied in the plate normal direction (ND), the direction that activates twinning the most (see Fig. 1(b) and (c)). The load cell of the stress rig measured the macroscopic stress in the sample, while the macroscopic strain was determined by monitoring the change in distance between two silver wires mounted on the ND/RD face of the sample. The wire positions were determined as the maxima in the fluorescent X-ray signal when scanning along the length of the sample. With the wire separation of 3.1 mm and a scanning step size of 5 μm the accuracy in the macroscopic strain was determined to be of the order of 3E-5 using Gaussian fitting of the fluorescent peak profiles. To have an independent measure of the strain, a resistive strain gauge was also glued onto the ND/RD face of the sample outside the investigated gauge volume. Our previous study on the same material indicated that the onset of macroscopic plasticity for this material is at $\varepsilon = 0.6\%$ [10], hence, measurements were carried out at seven different steps; one at an "unloaded" step, i.e. prior to loading, another in the elastic zone, one at the onset of macroscopic plasticity, and four in the plastic zone to monitor twin nucleation and thickening

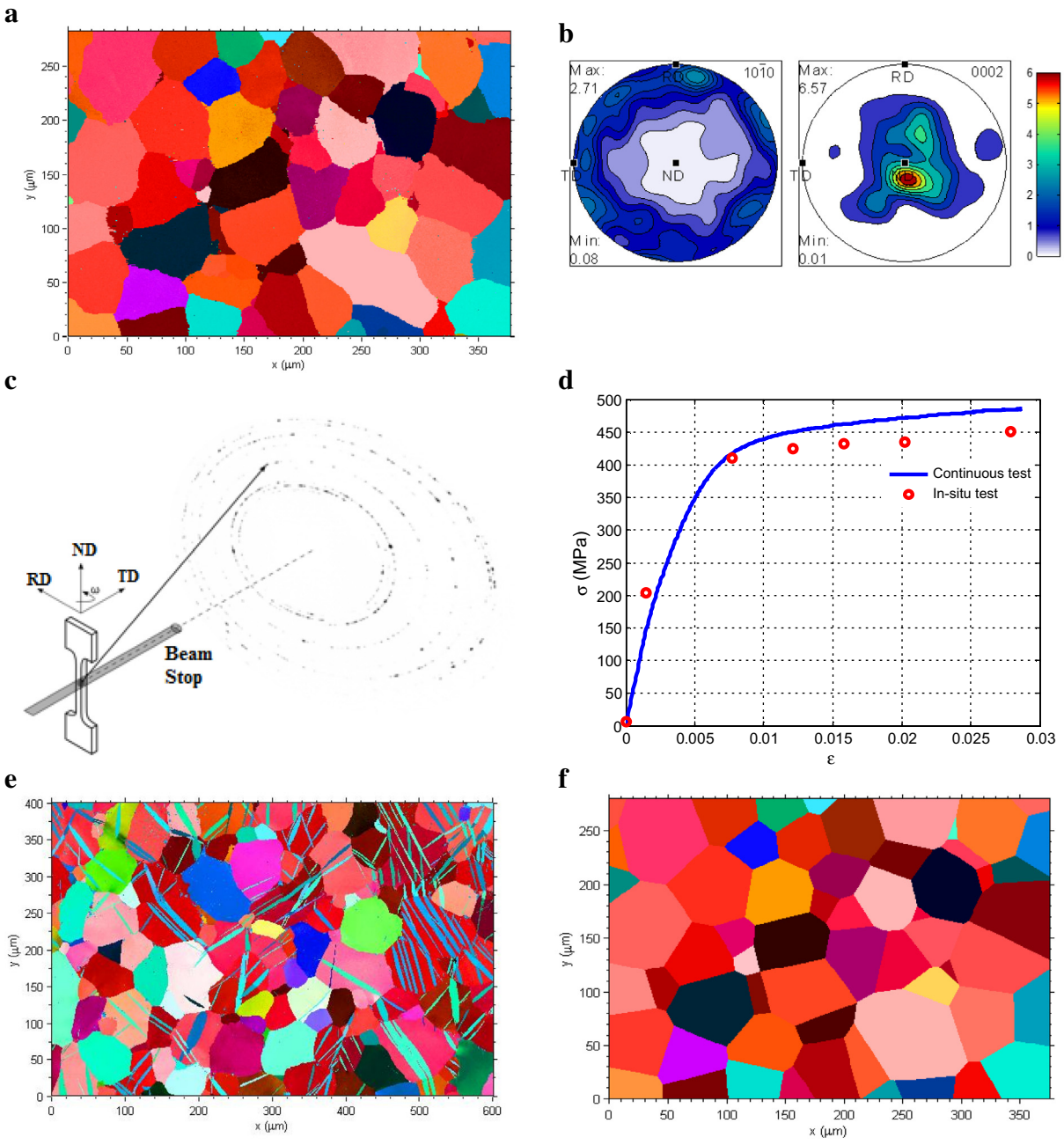

Fig. 1. (a) an EBSD map of the material used for 3DXRD; (b) pole figures of the same material; (c) a schematic of the experimental set-up and the sample used for 3DXRD; loading direction is along the ND axis as indicated; (d) flow curve for continuous loading of the material used for 3DXRD compared with the one measured during the *in-situ* experiment; (e) an EBSD map of the probed area *after* the 3DXRD experiment; (f) Weighted Voronoi estimation of the EBSD map shown in (a); same color coding is used.

(see Table 1 for more details). The sample was loaded under stress control in the elastic zone and strain control in the plastic zone with a strain rate $\dot{\varepsilon} = 5E-5s^{-1}$. Deformation was then stopped, and the sample held at constant strain. In the plastic zone, X-ray measurements for each step started only after the stress relaxed and reached a constant value (after approximately 20 min). The holding time for each measurement step is given in Table 1. The largest stress relaxation, which occurred for the last measurement step, was 50 MPa. A separate experiment was conducted to continuously measure the stress–strain curve without interruption (at same strain rate of 5E-5 1/s) and to compare against the one measured during the X-ray experiment. This is shown in Fig. 1(d).

The 3DXRD experiment was carried out by illuminating the volume of interest with a planar beam, which was initially defined by a slit to be 760 μm in the horizontal direction and 50 μm in the vertical direction (ND). The X-ray beam energy was calibrated to the Pt K-edge at 78.395 keV. By translating the sample with respect to the beam, the sample was probed in layers perpendicular to the tensile axis. To probe all grains in the illuminated

Table 1. Details of the results and error bars of the 3DXRD analysis.

Step	Macro-Strain%	Macro- Stress (MPa)	Data collection time (hours)	No. of Grains	No. of Twins	Diffraction spots per grain	Average grains error values			Stress Components (MPa)*		
							3-D position (μm)	Relative Volume%	Orientation (°)	ND	RD	TD
Step-1	0.00	6.5	12	6132	0	112	4	11	0.03	10 (30)	12 (12)	16 (−14)
Step-2	0.15	203.5	10	6104	12	112	4	12	0.03	10 (221)	11 (−5)	15 (−29)
Step-3	0.77	409.4	12	5975	11	104	5	16	0.03	12 (371)	14 (1)	19 (−12)
Step-4	1.21	424.1	15	7315	281	104	7	18	0.04	19 (389)	22 (39)	30 (31)
Step-5	1.58	432.3	15	7224	502	100	9	22	0.05	25 (395)	29 (40)	39 (35)
Step-6	2.02	435.3	20	8977	856	99	13	15	0.07	33 (389)	39 (51)	53 (46)
Step-7	2.79	451.1	24	9724	1054	91	17	20	0.09	46 (414)	54 (60)	74 (59)

* Average measured value for all of the grains is given in the parenthesis. Stress is applied along ND.

volume, and not just those that satisfy a single Bragg condition, the sample was rotated around the tensile axis and diffraction images were acquired in the angular range [−144°–−35°] and [36°–145°] in steps of 0.25°; the limits to the angular coverage are imposed by the pillars of the tensile stage. The diffraction images were collected on a Frelon2K detector where the exposure time throughout the experiment was constant at 0.25 s per image. The detector was placed at 0.37 m away from the sample to enable the detection of the first nine full Debye–Scherrer rings. The Frelon2K is a fast read out/ low noise detector which uses a multi-channel chip for fast read out and has 2048 × 2048 pixels [32]. As the sample is deformed, the number of diffraction peaks increases due to twinning, and the diffraction peaks smear out due to the induced internal orientation spread. To ensure that peaks can be separated as required for the reconstruction, the vertical dimension of the beam was slit down from initially 50 μm for strains less than 1% to 40 μm for strains between 1–2% and 20 μm for strains larger than 2%. Strain maps were collected at seven different load steps where at each load step, the number of consecutive layers was adjusted to cover at least 0.9 mm along the common tensile and rotation axis (see Fig. 1(c)). Details of the 3DXRD test set up for different load step are briefly shown in Table 1.

3. Analysis of the diffraction data

3.1. Detection and refinement of grains

The positions of the diffraction peaks were located using the peaksearch module from FABLE (http://sourceforge.net/apps/trac/fable/wiki). Thresholds for peaksearch were set at 50, 100, 200, 400, 800, 1600 and 3200 counts above the background level, after which a watershed-type merging algorithm was employed. Flood field and spatial distortion corrections were performed as part of the segmentation process. During the experiment the incident beam current ranged from 200 mA right after a refill of electrons into the synchrotron storage ring to 160 mA just before the next refill 12 h later. Therefore the intensities of all reflections were scaled to correspond to an incident beam current of 200 mA in order to put the grain volumes refined from peak intensities on an absolute scale.

The preliminary grain center-of-mass map was then reconstructed in an iterative procedure where GrainSpotter [33] was used to index grains from unassigned reflections, and make map from ImageD11 was employed to filter off the assigned reflections and produce a reflection list that could be recycled into GrainSpotter. The process is continued as long as new grains with at least 50% of the expected reflections are found within a tolerance of 0.02 in hkl during the indexing step. After this a test is carried out to ensure that none of the grains found in adjacent layers, or in the present layer at the previous load step, have been missed in the map. At the end of this procedure more than 90% of the reflections have been assigned to grains at strains below 1%, and more than 80% for the remaining load steps. FitAllB [22] was then run to simultaneously refine grain positions, orientations and strain tensors in each illuminated layer of the sample. The relative grain volumes were estimated from the intensities of the assigned reflections, taking the non-negligible absorption in the Zircaloy-2 sample at 78.395 keV into account. As a final

step the 2D layers were stacked in 3D using distance criteria of 0.07 mm and misorientation criteria of 1° between parts of the same grain distributed over adjacent layers in the illumination. The positions, orientations, strain and stress tensors for the resulting 3D grains are calculated as volume weighted averages over the corresponding 2D contributions. Table 1 gives statistics on the grains refined at each load step.

3.2. Grain labelling

The result from the analysis in Section 3.1 is grains that are independently labeled for each step, i.e. an identical grain in two different steps does not necessary have the same ID. In order to assign one unique ID to each grain that can be followed through the whole experiment, grains from each step were independently compared with those in Step-1 as well as their previous step. For this purpose, the center-of-mass of the probed volume at each step was calculated, and the effects of rigid body movement from step to step were eliminated by comparison to Step-1. Then for each step, the position and orientation of each grain were compared against all of the grains in Step-1. If two pair of grains, from Step-n and Step-1, have total misorientation as well as basal plane misorientation less than 5° and have less than 30 μm displacement, the same ID (label) was assigned to them. Since plastic deformation in some soft grains results in displacements of more than 30 μm in later steps, it is not possible to label these with the mentioned assumptions. This may happen especially if the grains are small and/or significantly deformed, resulting in weak diffraction spots that fall below the detection limit of the peaksearch. Further, twinning results in some new grains that cannot be labeled by comparing these newly born grains to grains from Step-1. Hence, an extra cross correlation between unlabeled grains in Step-n and those in Step-(n-1) was performed to ensure that twins or deformed grains are also labeled under the same ID. Finally if any grain remained unlabeled, a new ID was assigned to it.

3.3. Twin identification

The procedure described for defining annealing twins in copper using 3DXRD by Oddershede et al. [34] is adapted here for finding deformation twins. EBSD measurements on the annealed undeformed Zircaloy-2 sample have revealed that almost no twins exist prior to loading (see Fig. 1(a)). Hence, we assume that grains measured in Step-1, and followed under the same ID in the subsequent steps, can solely act as parent grains whereas new grains, first labeled in Step-2 to Step-7, can be twin candidates. As twins are indexed as 'new' grains, any two grains with distance between their center-of-mass positions less than the sum of their respective radii are candidates for being a twin and parent pair (see Fig. 1(e)). It is worth mentioning that the radius of each grain is calculated using Eq. (1);

$$V^g = V_R^g \times \frac{V^{TI}}{V^M} \tag{1}$$

where V^g represents the "actual" volume of grain g, V_R^g is the measured relative volume for grain g, V^{TI} is the total volume that was inspected and calculated based on the measured minimum and maximum in the center-of-mass positions, and V^M is the total volume measured for all of the inspected grains, i.e. summation over V_R^g for all inspected grains. It is assumed that the probed grains are space filling and there are no defects or missed grains in the probed volume.

For each step, once the candidate parent and twin pairs are identified, the misorientation between the normal to the basal planes of the pair and that of the twin habit planes in the parent and twin are calculated based on the measured orientation matrices. Since tension along the ND of Zircaloy-2 results in formation of tensile twins, if the basal misorientation is in the range of $85° \pm 5°$ and the habit plane misorientation is less than 5°, then the pair that fulfills these misorientation criteria is considered as a twin and parent pair. This method, in some cases, defines more than one parent grain to a twin, hence extra constraints are applied to define one unique parent grain to a twin. The results that are reported here are for parent and twin pairs that besides satisfying the described misorientation condition, have minimum distance, minimum misorientation in basal plane normal, and maximum local twin Schmid factor (see Section 4.3). This process is repeated independently for each step, i.e. the twin and parent pairs for Step-n are defined only by investigating grains in Step-n. Eventually the pairs that are successfully defined in more than *two independent steps* are considered as final twins and will be subsequently discussed here. While this therefore represents only a subset of the twins that will have formed in the material, it does mean that we have a high confidence of having successfully identified the twin with its true parent.

4. Results and discussion

Center-of-mass positions, orientations, volumes, elastic strains, and stresses of each individual grain along with associated error bars are outputs of the measurement for each loading. This is a lot of information, hence, selected results will be shown here and the observed trends will be explained. Also, for calculating stresses from measured elastic strains, the elastic constant of pure zirconium is used which is given by Fisher and Renken [35]: $C_{11} = 143.5$ GPa, $C_{33} = 164.9$ GPa, $C_{12} = 72.5$ GPa, $C_{13} = 65.4$ GPa, and $C_{44} = 32.1$ GPa.

4.1. Reconstructed volume

Two reconstructed maps from 3DXRD measurements for the unloaded and maximum load cases are shown in Fig. 2(a) and (c). Colors are coded with respect to the ND loading axis direction (see Fig. 2(b)) where the average measured orientation is compatible with the EBSD measurement shown in Fig. 1(b), i.e. the majority of grains have the *c*-axis oriented toward the loading direction, which is thus favorable for tensile twin formation under the stress applied. The size of the sphere representing each grain in Fig. 2 is proportional to the relative volume of the grain.

The number of measured grains and twins is reported in Table 1. As expected, the number of grains does not really change between Step-1 and Step-2 since no twins form. Step-3 is the onset of plasticity, and *in-situ* tensile experiments in SEM have indicated that it is also the onset of twin formation (at about $\varepsilon = 0.6\%$ [10]). However neither an *ex-situ* low resolution EBSD measurement nor the present 3DXRD measurement could capture twin formation at this stage. This is probably because the twins are less

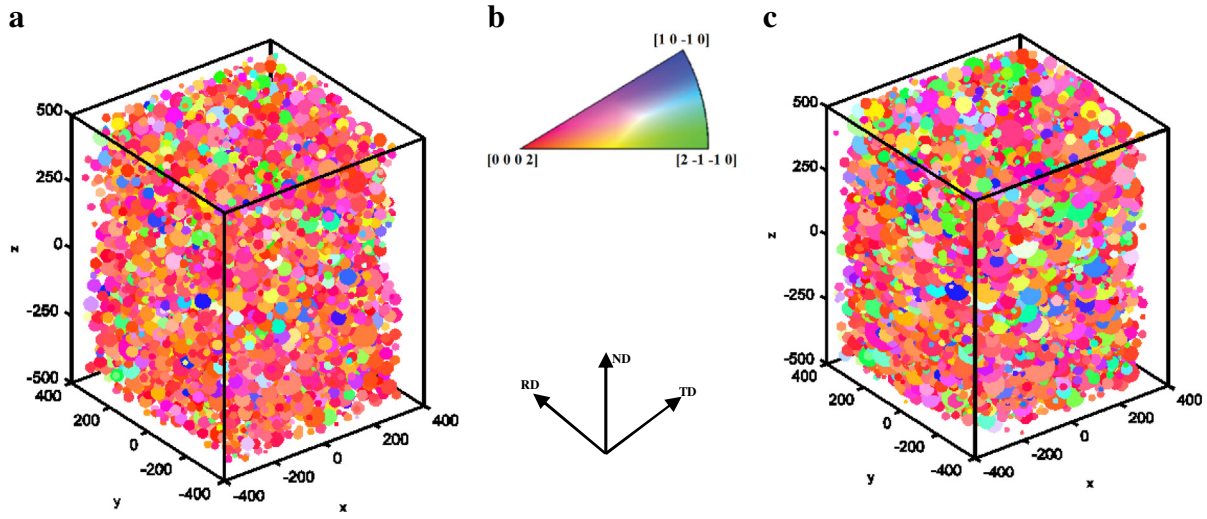

Fig. 2. Reconstructed 3D volume containing (a) 6132 grains for Step-1 and (c) 9724 grains for Step-7. The unit on the axes is μm. Colors are coded according to the Inverse Pole Figure in (b) that shows the crystallographic orientation of the grain along the tensile ND direction.

than a micron in thickness, although they are mostly long enough to intercept two grain boundaries; this small volume will make X-ray scattering from the twins relatively weak. Twin thickening then takes place between Step-4 and Step-7, accompanied by the formation of more twins. At $\varepsilon = 1.1\%$ the thickness of many of the twins is more than 3 μm, which is above the 3DXRD detection limit and the reason why the number of the grains is observed to increase in Step-4. In comparison to Step-4, the number of indexed grains is observed to slightly decrease in Step-5 although the same volume was probed. This will be due to plastic deformation and the smearing of diffraction spots, reducing the signal to noise and placing some grains below the detection threshold. Nevertheless, the number of twins has increased as expected. The formation of twins is also confirmed by reviewing the reconstructed 3D volume as in Fig 2(c), where more small green and blue grains, i.e. those with their basal plane normal perpendicular to the loading direction, are observed in comparison to the unloaded case.

It is worth mentioning that the filters applied for identifying twins will have led to missing many of the twins - at the benefit of having substantially higher confidence in associating the twins that are identified with their parent. As a consequence the number of twins reported in Table 1 are considerably lower than what can be observed using SEM/EBSD for this material [10]. Only about 11 twins are identified in Step-2 and Step-3 independently, which is acceptable since we know that a few twins do exist in our starting material (since it was rolled), and it is reasonable to assume that the recrystallization did not fully remove the twins (our subsequent EBSD measurements have confirmed this). The algorithm identified 1079 twins, of which 200 were formed at Step-4 and could be followed all the way through to Step-7. These twins are studied in detail in [26]. The number of parent grains that are assigned to the 1079 twins is 342, i.e. 3.1 twins per grain, where some of the grains have more than three twins and some of them have only one. In Fig. 1(e), an EBSD map of the area that was probed by synchrotron X-rays is illustrated, prepared after Step-7. The number of measured twins per grain in the scanned area using EBSD and 3DXRD are compatible. A previous statistical study of twins in pure zirconium using EBSD has indicated that the chance of having a grain twinned increases with the size of the grain, as does the number of twins per grain [16]. The average grain diameter of the Zircaloy-2 sample used in this experiment is 50 μm, and about half of the parent grains have diameters larger than this average value, which is also consistent with the EBSD observation.

4.2. Size effects

As we used grain sizes and orientations for identifying twin and parent pairs, it is essential to have an understanding of the distribution of both grain sizes and orientations. In order to shed more light on the trends observed in measured stresses for each step, measured Von Mises stresses are plotted against grain size and orientations. A $600 \times 600 \times 600\ \mu m^3$ cube containing more than 2700 grains located in the center of the probed volume are used to generate Figs. 3 and 4. The distribution of grain diameter measured in Step-1 is shown Fig. 3(a). The frequency of grains having average grain size (~50 μm) is the peak in the distribution, but more than 1500 grains are larger than the measured average grain size.

The measured Von Mises stress for each grain as a function of grain diameter for Step-4 and Step-5 are shown in Fig. 3(b) and (c). Not surprisingly, both the average and maximum stresses for each family of grain diameters reduce as the grain size increases. This phenomenon is generally known as the Hall–Petch effect, stating that coarse grained samples normally yield sooner than fine grained ones due to the presence of larger mean free paths for dislocation movement. Also, the number of neighboring grains normally increases with an increase in grain size, and hence so does the probability of having a hard neighboring grain that can cause early yield, due to load sharing with a softer coarse grain. As coarse- grained Zircaloy-2 hardens with a gentle slope (i.e. low work hardening), the range of stress variations stays almost the same for the steps indicated. This is also reflected in the average stress strain curve shown in Fig. 1d. Further, although the average stress in

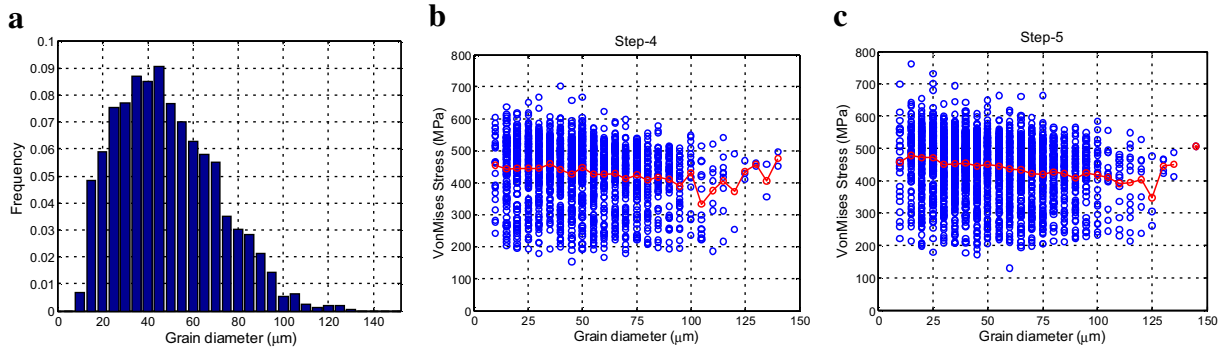

Fig. 3. Grain size effect on the Von Mises stress distribution: (a) grain size distribution; Von Mises stress measured in (b) Step-4 and (c) Step-5 as a function of grain diameter. Red lines in (b) and (c) indicate the average value. (For interpretation of the references to color in this figure legend, the reader is referred to the web version of this article.)

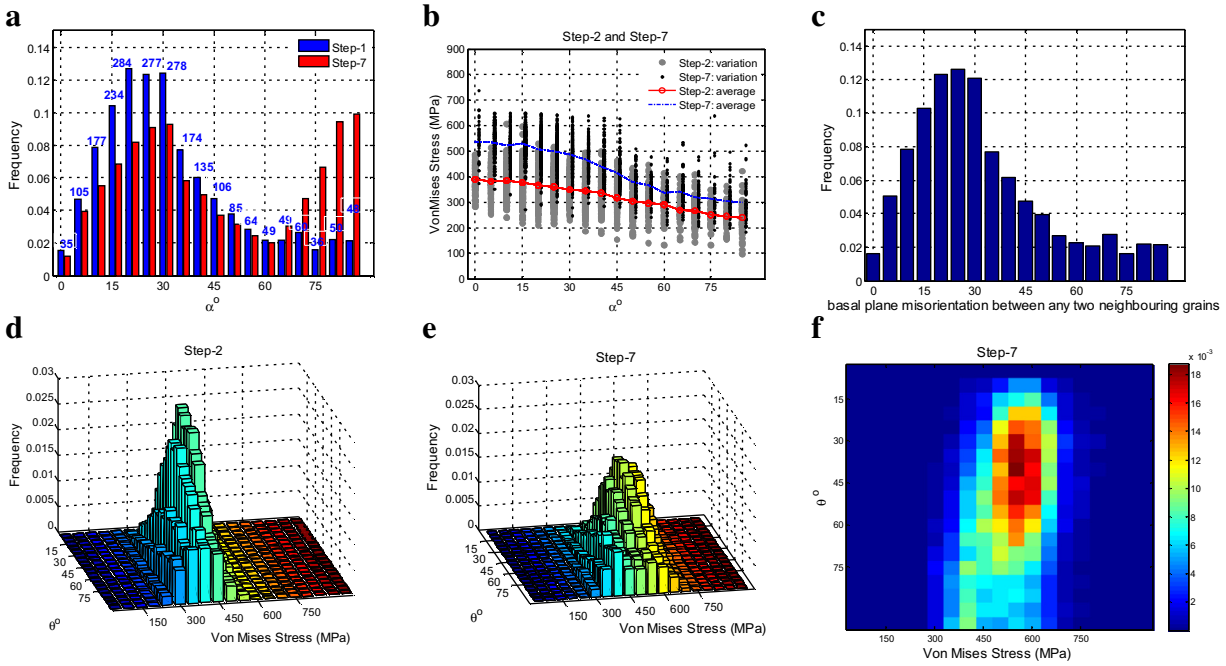

Fig. 4. Effect of misorientation on the stress development; (a) distribution of misorientation between the basal plane normal and the loading direction (α^o) for grains measured in Step-1 and Step-7. The number of observation for each angular range in Step-1 is indicated above the data set; (b) Von Mises Stress as a function of α for Step-2 and Step-7; (c) distribution of the misorientation between the basal plane normal ($\theta°$) of any two neighboring grains measured in Step-1; distribution of Von Mises Stress as a function of θ for (d) Step-2 and (e) Step-7; (f) a top-view contour plot of the results shown in (e).

Fig. 3(b) and (c) (red line) stays somewhere between 400–500 MPa, a rather wide variation about this mean value is observed in individual grains. This distribution of stresses reflects the effects of orientation and neighborhood, coupled with the high anisotropy in elastic and plastic properties of Zircaloy-2.

4.3. Orientation effect

Two different parameters that reflect the effects of average and local misorientation are used to study the evolution of stress within the probed volume. In Fig. 4(a) the frequency of misorientation between basal plane normal and loading direction (α) for the grains measured in Step-1 and Step-7 is illustrated. As the sample is highly textured (Fig. 1(b)), most of the parent grains have basal plane normals aligned with the loading direction ($\alpha < 30°$). These are plastically 'hard' grains since they have low basal and prism (i.e. easy) slip activity. With more deformation at Step-7, the population of grains at $\alpha > 65°$ increases, which is due to tensile twin formation.

The stress distribution in each grain as a function of α for the elastic Step-2 and plastic Step-7 are shown in Fig. 4(b). As elastic deformation is the dominant deformation mechanism in Step-2, the variations here are mostly controlled by elastic anisotropy and the orientation of grains. In contrast, in Step-7 both elastic and plastic anisotropy play a role. The average stress in Step-2 varies from 375 MPa to 235 MPa depending on grain orientation, while in Step-7 it varies from 520 MPa to 300 MPa, i.e. higher stress values are obtained due to hardening, while a wider

range of stresses reflects the effects of plastic anisotropy / plasticity induced load sharing. The influence of neighboring grains can be clearly seen in Step-7 where for $\alpha > 60°$, high stresses are present in many grains above the blue (average) line that, based on their orientation, should have an easy slip system available, yet they act like 'plastically hard' grains. More detailed information on the effect of neighboring grains can be extracted by investigating the local misorientation between any two neighboring grains (Fig. 4(c)).

In order to define the neighbors of each grain, a weighted Voronoi method is used to construct a 3D space-filling map of the grains based on the measured center-of-mass position and volume of each grain. Details of the method are given in [36] and its application for constructing 3D maps is given in [26,37]. In order to validate the code that we developed and as an example of how well neighbors of a grain can be identified, as well as how grain boundaries can be simulated, the measured EBSD map shown in Fig. 1(a) is reconstructed using the center-of-mass positions as well as the area fractions of each grain. Generally a 3D code cannot be convincingly validated with a 2D demonstration, but this direct comparison between a reconstructed map and the real microstructure shown in Figs 1(f) and (a), respectively, suggests that the approach can be effective. This code was then used to construct 3D grain geometries and to identify probable neighbors for each grain. On average, each grain has ~12 neighboring grains, larger grains have more neighbors while smaller grains have fewer.

The distribution of the misorientation between the basal planes of any two neighboring grains (θ) for Step-1 is shown in Fig. 4(c). As the material is highly textured, most of the neighbors have $\theta < 30°$. The three-dimensional distribution of Von Mises stresses as a function of θ for Step-2 and Step-7 are illustrated in Fig. 4(d) and (e), respectively. Prior to plastic deformation, the peaks in the Step-2 distribution are higher and sharper than those in Step-7. Further, at lower Von Mises stresses, the peaks in the distribution tend to appear toward the high angle of the θ-axis while at higher Von Mises stresses they appear toward the low angle of the θ-axis, i.e., soft grains with a low level of stress are surrounded by many hard grains. This is why a peak is observed at θ~75° in both Step-2 and Step-7. In Fig. 4(f), (a) clearer picture of the position of the maximum values is given via a top-view contour plot of the results shown in Fig. 4(e).

4.4. Variant selection and twin Schmid factor

Tension along the c-axis of an hcp crystal will potentially activate six different variants of the $\{10\bar{1}2\}\langle 10\bar{1}0\rangle$ tensile twinning system. Depending on the local stress state, which is strongly influenced by the misorientation between the c-axis and the loading direction, the probability of different twin variants forming will be altered. We term the twin variant that is most favoured by a particular average stress state the 'favored variant'. It is crucial to understand the mechanism of variant selection, as preference in selection of one variant would result in a noticeable macroscopic shape change and/or accommodation of applied stress.

In this section we determine whether the habit plane identified for each twin and parent pair in Section 3.3 corresponds to the most favored variant. For this purpose, once a twin is discerned for the first time, the Schmid factors of all the possible variants are calculated based on the grain orientation and the global applied stress; we term this the Global Schmid Factor (GSF). Similarly the Schmid factors based on the average stress over the whole grain measured using 3DXRD will be called the Average Local Schmid Factor (ALSF). It should be noted that the Schmid factor calculated for different locations inside a grain, can vary significantly compared to the ALSF [26,37]. As the stress state inside the parent grain is tri-axial, the following formulation is used to calculate the Schmid factors [10,38]:

$$SF^{\beta} = \frac{P^{\beta} : \sigma}{\|\sigma\|} \tag{2}$$

where SF^{β} represents the Schmid factor of twin variant β, and $\|\sigma\|$ is the norm of the stress tensor (highest value between absolutes of the principal stresses), and P^{β} is the symmetric part of the Schmid tensor of the twin variant β. In this definition, depending on the state of the triaxial stress and crystal orientation, SF^{β} can be as high as one. Once GSF and ALSF of each twin variant are calculated, they are sorted from maximum to minimum, i.e. rank one is assigned to the most favored variant and six to the least favored variant, and the rank of the variant that has actually occurred is identified. In Fig. 5(a) the contribution of each variant to the 1079 identified twins is shown. For the GSF, the number fraction of each variant decreases as the variant becomes weaker, yet not all of the twins are formed based on the most favored variant. This

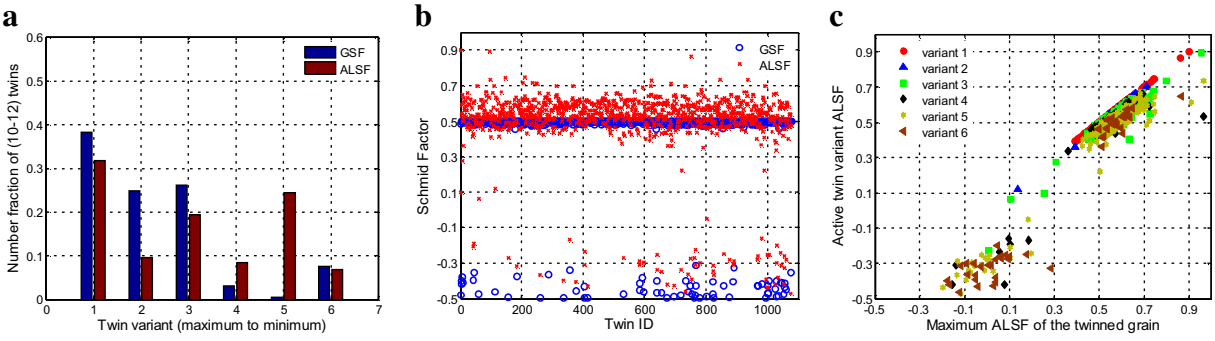

Fig. 5. (a) Number fraction of each twin variant ordered from highest to lowest twin Schmid factor. (b) Global (GSF) and average local Schmid factor (ALSF) of each individual twin. (c) Average local twin Schmid factor of the active variant as a function of the maximum average local twin Schmid factor in the corresponding parent grain. The measured tri-axial stress within each parent grain is used for calculating ALSF.

phenomenon is also reported from EBSD analysis on twins in Zr [16] and Mg [17]. As the material is highly textured and the *c*-axis in most of the grains are aligned toward the loading direction (Fig. 4(a)), there is strong competition between the six variants, and based on the GSF they all have Schmid factors close to 0.5, so there is no significantly favored variant. Although the first variant ordered based on ALSF contributes the most twins, the number fraction of less favored variants is greater than that observed when ranking with the GSF. In order to gain a better insight into this, the calculated GSF and ALSF for the variant that caused twinning is shown in Fig. 5(b). More than 88% of the identified twins have ALSF larger than 0.45, so these grains are very well aligned for twinning, i.e. the misorientation between basal plane normal and loading direction for these grains is small. This indicates that there is a strong competition between all of the variants inside the twinned grains, and that the variant selection is controlled rather by local effects that could not be captured by the spatial resolution used in 3DXRD. This is also supported by finite element modeling [26,37]. Interestingly, about 6% of the identified twins, with an ALSF and GSF significantly lower than zero, have parent grains that are not favorably aligned for twinning, which suggests that deformation in a neighboring grain could be responsible for triggering twins in these grains. Besides the fact that soft grains are surrounded by many hard grains, which can significantly influence twin nucleation in soft grains (Fig. 4), EBSD analysis and crystal plasticity modeling of the same material have also demonstrated this phenomenon [10]. In order to have a better understanding of variant selection in both low Schmid factor and high Schmid factor twins, the ALSF of each active variant is plotted against the maximum ALSF calculated for each corresponding parent grain; results are shown in Fig. 5(c). In the grains that are favorably aligned for twinning all of the six variants are active, however, less favored variants are active in the soft parent grains (i.e., those unfavorably aligned for twinning). Some extremely low 'unfavorable' twins are seen to nucleate even when a moderately high maximum ALSF is available, demonstrating that local neighborhood dominates in these cases; e.g., consider for instance values of maximum ALSF in the range 0.1 to 0.3, where active twin variants have ALSF as low as −0.3.

5. Conclusion

An *in-situ* three-dimensional synchrotron X-ray diffraction experiment was carried out on a sample made of coarse grained Zircaloy-2. The sample was uni-axially strained up to 2.7% in seven steps in the direction relative to the texture that activates twinning the most. Due to elastic anisotropy, orientation and neighborhood effects, the average measured stress within each grain was found to vary significantly compared to the measured average stress value, even in the elastic zone. As a result of twinning, the number of grains in the probed volume increased with higher strain levels. An algorithm was adopted to define twins and parent grain using many credibility filters, and the 1079 twins from 342 parents that could pass all of the filters were studied statistically.

For the first time, a statistical analysis of the experimental 3D stress state is made during twinning, connecting twins to their parents through multiple deformation steps. It is shown that both plastically soft and plastically hard grains are twinned, and that a strong competition between the six possible variants exists inside hard grains, which are favorably oriented for twinning. In terms of twin variant selection, it is shown that if variants are ordered from highest to lowest Global Schmid factor, the number fraction of observed variants decreases with Schmid factor. On the other hand, if they are ordered based on the Average Local Schmid factor, although the most favored variant contributes the largest fraction of twins, the fraction of all the lesser favored variants is greater than is observed using the Global Schmid factor; this demonstrates the influence of neighboring grains. Furthermore, twin formation is observed in soft grains which are poorly oriented for twinning; this reflects the effect of deformation in the many hard neighboring grains that surround each soft grain. In these grains that are poorly oriented for twinning, twin variants occur that are extremely unfavored based on either the Global or Average Local Schmid factor.

Acknowledgements

This work was supported by a Discovery Grant from the Canadian Natural Sciences and Engineering Research Council. The authors acknowledge the ESRF for allocating beam time for experiment MA-1213. Financial support from the Danish Council for Independent Research via Danscatt is appreciated. HA is also grateful to the Engineering and Physical Sciences Research Council (EP/K034332/1) for financial support.

References

[1] F. Xu, R.A. Holt, M.R. Daymond, J. Nucl. Mater. 394 (2009) 9.
[2] H. Abdolvand, M.R. Daymond, C. Mareau, Int. J. Plast. 27 (2011) 1721.
[3] B.C. Ng, B.A. Simkin, M.A. Crimp, T.R. Bieler, Intermetallics 12 (2004) 1317.
[4] T.R. Bieler, A. Fallahi, B.C. Ng, D. Kumar, M.A. Crimp, B.A. Simkin, A. Zamiri, F. Pourboghrat, D.E. Mason, Intermetallics 13 (2005) 979.
[5] J. Oddershede, B. Camin, S. Schmidt, L.P. Mikkelsen, H.O. Sørensen, U. Lienert, H.F. Poulsen, W. Reimers, Acta Mater. 60 (2012) 3570.
[6] M. Kerr, M.R. Daymond, R.A. Holt, J.D. Almer, Acta Mater. 58 (2010) 1578.
[7] K. Pettersson, J. Nucl. Mater. 56 (1975) 91.
[8] A. Stoll, A.J. Wilkinson, Comput. Mater. Sci. 89 (2014) 224.
[9] F.P.E. Dunne, Curr. Opin. Solid State Mater. Sci. 18 (4) (2014) 170.
[10] H. Abdolvand, M.R. Daymond, J. Mech. Phys. Solids 61 (2013) 803.
[11] H. Wang, P.D. Wu, J. Wang, C.N. Tomé, Int. J. Plast. 49 (2013) 36.
[12] C.C. Aydıner, M.A. Telemez, Int. J. Plast. 56 (2014) 203.
[13] L. Balogh, S.R. Niezgoda, A.K. Kanjarla, D.W. Brown, B. Clausen, W. Liu, C.N. Tomé, Acta Mater. 61 (2013) 3612.
[14] C.C. Aydıner, J.V. Bernier, B. Clausen, U. Lienert, C.N. Tomé, D.W. Brown, Phys. Rev. B 80 (2009) 024113.
[15] T. Bieler, L. Wang, A. Beaudoin, P. Kenesei, U. Lienert, Metall. Mater. Trans. A 45 (2014) 109.
[16] L. Capolungo, P.E. Marshall, R.J. McCabe, I.J. Beyerlein, C.N. Tomé, Acta Mater. 57 (2009) 6047.
[17] I.J. Beyerlein, L. Capolungo, P.E. Marshall, R.J. McCabe, C.N. Tomé, Philos. Mag. 90 (2010) 2161.

[18] B. Clausen, C.N. Tomé, D.W. Brown, S.R. Agnew, Acta Mater. 56 (2008) 2456.
[19] O. Muránsky, M.R. Daymond, D. Bhattacharyya, O. Zanellato, S.C. Vogel, L. Edwards, Mater. Sci. Eng. A 564 (2013) 548.
[20] R.Y. Zhang, M.R. Daymond, R.A. Holt, Mater Sci. Eng. A 473 (2008) 139.
[21] H.F. Poulsen, Three-Dimensional X-ray Diffraction Microscopy: Mapping Polycrystals and their Dynamics, Springer, Berlin, 2004.
[22] J. Oddershede, S. Schmidt, H.F. Poulsen, H.O. Sorensen, J. Wright, W. Reimers, J. Appl. Crystallogr. 43 (2010) 539.
[23] W. Ludwig, S. Schmidt, E.M. Lauridsen, H.F. Poulsen, J. Appl. Crystallogr. 41 (2008) 302.
[24] W. Ludwig, A. King, P. Reischig, M. Herbig, E.M. Lauridsen, S. Schmidt, H. Proudhon, S. Forest, P. Cloetens, S. Rd Roscoat, J.Y. Buffière, T.J. Marrow, H.F. Poulsen, Mater. Sci. Eng. A 524 (2009) 69.
[25] P. Reischig, A. King, L. Nervo, N. Vigano, Y. Guilhem, W.J. Palenstijn, K.J. Batenburg, M. Preuss, W. Ludwig, J. Appl. Crystallogr. 46 (2013) 297.
[26] H. Abdolvand, M. Majkut, J. Oddershede, J. Wright, M.R. Daymond, Acta Mater. 93 (2015) 235.
[27] Abaqus. Standars user's manual version 6.5: Habitt. Karrlsson & Sorensen Inc, 2005.
[28] H. Abdolvand, M.R. Daymond, J. Mech. Phys. Solids 61 (2013) 783.
[29] F. Xu, R.A. Holt, M.R. Daymond, R.B. Rogge, E.C. Oliver, Mater. Sci. Eng. A 488 (2008) 172.
[30] C. Mareau, M.R. Daymond, Acta Mater. 58 (2010) 3313.
[31] S.R. MacEwen, J. Faber Jr, A.P.L. Turner, Acta Metall. 31 (1983) 657.
[32] J.-C. Labiche, O. Mathon, S. Pascarelli, M.A. Newton, G.G. Ferre, C. Curfs, G. Vaughan, A. Homs, D.F. Carreiras, Rev. Sci. Instrum. 78 (2007).
[33] S. Schmidt, J. Appl. Crystallogr. 47 (2014) 276.
[34] J. Oddershede, S. Schmidt, H.F. Poulsen, L. Margulies, J. Wright, M. Moscicki, W. Reimers, G. Winther, Mater. Charact. 62 (2011) 651.
[35] E.S. Fisher, C.J. Renken, Phys. Rev. B 135 (1964) 482.
[36] A. Lyckegaard, E.M. Lauridsen, W. Ludwig, R.W. Fonda, H.F. Poulsen, Adv. Eng. Mater. 13 (2011) 165.
[37] H. Abdolvand, M. Majkut, J. Oddershede, S. Schmidt, U. Lienert, B. Diak, P.J. Wither, M.R. Daymond, On the deformation twinning of Mg AZ31B: A three-dimensional synchrotron X-ray diffraction experiment and crystal plasticity finite element model, Int. J. Plasticity 70 (2015) 77.
[38] I.J. Beyerlein, C.N. Tomé, Proc. Royal Society A: Math., Phys. Eng. Sci. 466 (2010) 2517.